Published in final edited form as:
Circulation. 2014 January 21; 129(3): 359–372. doi:10.1161/CIRCULATIONAHA.113.003000.

Vascular Progenitors from Cord Blood-Derived iPSC Possess Augmented Capacity for Regenerating Ischemic Retinal Vasculature

Tea Soon Park, PhD[1,*], **Imran Bhutto, MD, PhD**[2,*], **Ludovic Zimmerlin, PhD**[1], **Jeffrey S. Huo, MD, PhD**[1], **Pratik Nagaria, PhD**[3], **Diana Miller, BS**[4], **Abdul Jalil Rufaihah, PhD**[5,6], **Connie Talbot, BS**[7], **Jack Aguilar, BS**[1], **Rhonda Grebe, BS**[2], **Carol Merges, MA**[2], **Renee Reijo-Pera, PhD**[6], **Ricardo A. Feldman, PhD**[4], **Feyruz Rassool, PhD**[3], **John Cooke, PhD**[5,6], **Gerard Lutty, PhD**[2,†], and **Elias T Zambidis, MD, PhD**[1,†]

[1]Institute for Cell Engineering, and Kimmel Comprehensive Cancer Center, Johns Hopkins School of Medicine, Baltimore, MD

[2]Wilmer Ophthalmological Institute, Johns Hopkins University School of Medicine, Baltimore, MD

[3]Department of Radiation Oncology, University of Maryland School of Medicine, Baltimore, MD

[4]Department of Microbiology/Immunology, University of Maryland School of Medicine, Baltimore, MD

[5]Department of Cardiovascular Medicine, Stanford University, Palo Alto, CA

[6]Institute for Stem Cell Biology and Regenerative Medicine, Stanford University, Palo Alto, CA

[7]Institute for Basic Biomedical Science at Johns Hopkins School of Medicine, MD

Abstract

Background—The generation of vascular progenitors (VP) from human induced pluripotent stem cells (hiPSC) has great potential for treating vascular disorders such as ischemic retinopathies. However, long-term *in vivo* engraftment of hiPSC-derived VP into retina has not yet been reported. This goal may be limited by the low differentiation yield, greater senescence, and poor proliferation of hiPSC-derived vascular cells. To evaluate the potential of hiPSC for treating ischemic retinopathies, we generated VP from a repertoire of viral-integrated and non-integrated fibroblast and cord blood (CB)-derived hiPSC lines, and tested their capacity for homing and engrafting into murine retina in an ischemia-reperfusion (I/R) model.

Methods and Results—VP from human embryonic stem cells (hESC) and hiPSC were generated with an optimized hemato-vascular differentiation system. FACS-purification of human

Correspondence: Elias T. Zambidis MD, PhD, Institute for Cell Engineering and Kimmel Comprehensive Cancer Center, The Johns Hopkins University School of Medicine, 733 N. Broadway, MRB 755, Baltimore, MD 21205, Phone: 410-502-7519, Fax: 443-287-5611, ezambid1@jhmi.edu.
*contributed equally
†Co-senior authors

Conflict of Interest Disclosures: Under a licensing agreement between Life Technologies and the JHU, ETZ is entitled to a share of royalty received by the University for licensing of stem cells. The terms of this arrangement are managed by JHU in accordance with its Conflict of Interest policies. This does not alter the authors' adherence to journal policies on sharing data and materials.

embryoid body (hEB) cells differentially expressing endothelial/pericytic markers identified a $CD31^+$ $CD146^+$ VP population with high vascular potency. Episomal CB-iPSC generated these VP with higher efficiencies than fibroblast-iPSC. Moreover, in contrast to fibroblast-iPSC-VP, CB-iPSC-VP maintained expression signatures more comparable to hESC-VP, expressed higher levels of immature vascular markers, demonstrated less culture senescence and sensitivity to DNA damage, and possessed fewer transmitted reprogramming errors. Luciferase transgene-marked VP from hESC, CB-iPSC, and fibroblast-iPSC were injected systemically or directly into the vitreous of retinal I/R-injured adult NOD-SCID mice. Only hESC- and CB-iPSC-derived VP reliably homed and engrafted into injured retinal capillaries, with incorporation into damaged vessels for up to 45 days.

Conclusions—VP generated from CB-iPSC possessed augmented capacity to home, integrate into, and repair damaged retinal vasculature.

Keywords

Human induced pluripotent cells; embryonic stem cells; progenitor; endothelial differentiation; vasculature; retinopathy; ischemia-reperfusion; transplantation

Introduction

The human retina's high metabolism makes it uniquely reliant on an intact, functional vasculature. Photoreceptors consume the highest amount of oxygen per gram of tissue in the body, and thus require a continuous source of oxygenated blood. The human ophthalmic artery supplies twenty percent of its blood to the retina and ~80% to the choroid and uveal tract. If either the retinal or choroidal vasculature becomes compromised, neurons in affected ischemic areas rapidly die. Following branch vein occlusion (BVO)[1,2] and during the course of diabetic retinopathy (DR)[3–5], ischemia results in retinal pericyte and endothelial cell (EC) death. This leads to acellular vascular segments, rapid death of retinal neurons, secondary inflammation[6–8], and further retinal damage from subsequent compensatory neovascularization[9–13]. In both BVO and DR, the regeneration of retinal capillaries with cellular therapies using vascular progenitors (VP) could reverse the ischemic death of retinal neurons as well as associated secondary pathological neovascularization, thus potentially ameliorating or preventing end stage blindness.

Several groups have demonstrated the feasibility of regenerating ischemic retinal vasculature with cellular therapies. For example, transplanted adult hemato-endothelial[11,12,15] or embryonic hemangioblastic[14] progenitors were shown to home to degenerated ocular vascular sites created by severe ischemia or long-term diabetes. However, adult VP are rare in circulating peripheral blood and bone marrow, and restricted in expansion capacities. Furthermore, adult VP from diabetics are limited in their regenerative potential since they are functionally defective due to chronic hyperglycemia[16,17]. The regeneration of highly proliferative embryonic VP from patient-specific or HLA-defined hiPSC would circumvent these caveats and provide unlimited sources of pristine, non-diseased progenitors for cellular therapies.

The ability of hPSC to differentiate into vascular-endothelial progenitors with *in vivo* engraftment potential has previously been demonstrated[18–23]. Additionally, both adult and hESC-derived hemangioblasts possessing endothelial capacities could transiently populate injured tissue, including the retina[14,24–26]. However, long-term and functional *in vivo* engraftment of hiPSC-derived vascular cells has not yet been reported in the retina. Additionally, the use of viral vectors for expressing reprogramming factors in somatic cells poses a major obstacle limiting clinically useful hiPSC-based vascular therapies. Despite overall silencing of integrated retroviral and lentivector promoters during hiPSC generation, low levels of viral transgenes or reactivated vector promoters can result in incompletely-reprogrammed states that can promote insertional mutagenesis or malignant transformation[27,28]. Additionally, many standard hiPSC lines have differentiated to the vascular lineage with poor efficiency, more rapid senescence, and reduced proliferation rates compared to hESC[29]. It is currently unknown whether hiPSC made with non-integrated methodologies[30–32] will have similar or fewer limitations for generating therapeutically useful vascular lineages.

We recently described an efficient method for generating non-integrated hiPSC from human myeloid progenitors, including from cord blood (CB)[31,32]. These high-fidelity (HF) CB-iPSC lines possessed global and pluripotency-associated transcriptional signatures that were indistinguishable from hESC[32]. We also recently described methods for generating hemato-vascular progenitors from an optimized differentiation system[33,34]. Here, we demonstrate that VP differentiated from non-integrated HF CB-iPSC possess an enhanced potential for repairing damaged retinal blood vessels in a pre-clinical ischemic retinopathy model.

Methods

Detailed Expanded Methods are available in the Online-only Data Supplement.

Ethics Statement

The hESC lines H1 (WA01), H7 (WA07), H9 (WA09), and ES03 (ES03) used in these studies were obtained from the Wisconsin International Stem Cell Bank (WISCB). The use of all WISCB-donated hESC lines in these studies was approved by the Johns Hopkins Institutional Stem Cell Research Oversight (ISCRO) and Institutional Review Board (IRB) Committees. All animal surgical procedures were performed in accordance with protocols approved by the Johns Hopkins School of Medicine Institute of Animal Care and Use Committee (IACUC) and the Association for Research of Vision and Ophthalmology statement for the Use of Animals in Ophthalmic and Visual Research.

Isolation of hEB-Derived VP Populations Expressing CD31 and CD146

Our vascular differentiation system was previously described[24,33,35], and is summarized in Figure 1A. Recipes for all differentiation reagents, antibodies, and PCR primers are provided in Tables S1–S7. Briefly, day 8 hEB were disaggregated using collagenase type-IV (1mg/mL, Sigma-Aldrich, St. Louis, MO), and plated onto fibronectin (10 μg/mL, Life Technologies, Grand Island, NY)-coated plates in endothelial growth medium-2 (EGM2, Lonza, Walkersville, MD) supplemented with 25 ng/mL of $VEGF_{165}$ (Peprotech, Rocky

Hill, NJ). Four to six days later, adherent hEB-derived cells were treated with 0.05% trypsin-EDTA (Life Technologies) for 5 min at 37°C, and washed in mouse embryonic fibroblast (MEF) medium (Table S2). Cell clumps were filtered using a 40μm cell-strainer (Fisher Scientific, Pittsburgh, PA), centrifuged at 200g for 5 min, and resuspended at a concentration of 1×10^7 cells/mL in EGM2/PBS (1:1) solution. Fluorescence-activated cell sorting (FACS) was conducted at the Johns Hopkins FACS Core Facility with a FACS Aria III instrument (BD Biosciences, San Jose, CA). Cell suspensions were incubated with mouse anti-human CD31-APC (eBioscience, San Diego, CA) and CD146-PE (BD Biosciences) antibodies for 30 min on ice, FACS-purified into four fractions based on high CD31 and CD146 expression (Figure 1B), plated onto fibronectin-coated plates in EGM2, and expanded to 80–90% confluency for 7–9 days prior to *in vivo* injections.

Ocular Ischemic Reperfusion (I/R) Injury and Human Cell Injections

Four- to six-week old male NOD-SCID mice (Jackson Laboratory, Bar Harbor, ME) were subjected to high intraocular pressure to induce retinal ischemia-reperfusion injury. Mice were deep anesthetized by intraperitoneal (IP) injection of ketamine/xylazine (50 mg/kg ketamine + 10 mg/kg xylazine in 0.9% NaCl). The pupils were dilated with 2.5% phenylephrine hydrochloride ophthalmic solution (AK-DILATE, Akorn, Buffalo Glove, IL) followed by 0.5% tetracaine hydrochloride ophthalmic topical anesthetic solution (Phoenix Pharmaceutical, St. Joseph, MO). The anterior chamber of the eye was cannulated under microscopic guidance (OPMI VISU 200 surgical microscope (Zeiss, Gottingen, Germany) with a 30-gauge needle connected to a silicone infusion line providing balanced salt solution (Alcon Laboratories, Fort Worth, TX); avoiding injury to the corneal endothelium, iris, and lens. Retinal ischemia was induced by raising intraocular pressure of cannulated eyes to 120 mmHg for 90 min by elevating the saline reservoir. Ischemia was confirmed by iris whitening and loss of the retinal red reflex. Anesthesia was maintained with two doses of 50 μL intramuscular ketamine (20 mg/mL) during the 90 min. The needle was subsequently withdrawn, intraocular pressure normalized, and reperfusion of the retinal vessels confirmed by reappearance of the red reflex. The contralateral eye of each animal served as a non-ischemic control. Antibiotic ointment (Bacitracin zinc and Polymyxin B sulfate, AK-Poly-Bac, Akron) was applied topically. Two days later, FACS-purified human VP were injected into either the vitreous body (50,000 cells in 1 μL/eye), the orbital sinus (100,000 cells in 2 μL/eye; using a micro-injector (PLI-100, Harvard Apparatus, Holliston, MA), or into the tail vein (300,000 cells/100 μL/mouse).

Statistics

To evaluate statistical significance, two-tailed t tests (between individual groups), or one-way analysis of variance (e.g., ANOVA-Eisenhart's method with Bonferroni correction for three or more groups) were performed. For smaller, non-Gaussian-distributed sample sizes ($n<10$), nonparametric (Mann-Whitney) tests were performed. P values <0.05 or <0.01, respectively, were considered significant.

Microarray Accession

The NIH Gene Expression Omnibus has issued the accession number GSE44926.

Results

Enrichment of a VP Population Differentiated from hPSC with Enhanced *in Vitro* and *In Vivo* Vascular Pericytic-Endothelial Potential

We previously described a differentiation system that generated mesodermal-hemato-endothelial and CD143/ACE$^+$ hemangioblast progenitors from hPSC[24]. We recently optimized this system to generate hemato-vascular progenitors (Figure 1A)[33,34]. To identify a putative embryonic VP population, we expanded day 8 hEB cells for 4–6 days in EGM2 cultures supplemented with $VEGF_{165}$ (Figure S1), and subdivided adherent CD31$^+$ cells by their co-expression of the endothelial-perivascular-mesenchymal stem/progenitor (MSC) marker CD146[22,36,37] (Figure 1B, Figure S2, S3). Four populations were FACS-purified from adherent cells (CD31$^+$ CD146$^-$, CD31$^+$ CD146$^+$, CD31$^-$ CD146$^-$, and CD31$^-$ CD146$^+$), further expanded in EGM2 medium, and analyzed for surface co-expression of established hemato-endothelial, mesenchymal, pericytic, and smooth muscle cell markers (Figures S3–S5). Fractionating CD31$^+$ vascular-endothelial populations for high co-expression of CD146$^+$ enriched a putative VP population that that co-expressed mesenchymal stem cell (MSC) markers (CD44, CD90, CD105; Figure S3), the hemato-endothelial progenitor marker CD117 (C-KIT; Figure S5), but lacked hematopoietic-myeloid (Figure S6) or smooth muscle (α-SMA-positive; Figure S4) potential. Further EGM2 expansion of purified CD31$^+$ CD146$^+$ VP generated two discrete cellular phenotypes: an endothelial progenitor cell (EPC)-like (CD105^{hi}CD144$^+$CD140b$^-$) population, and a pericytic-like (CD31$^-$CD105^{dim}CD144$^-$CD140b$^+$) population (Figure S7).

To evaluate the endothelial functionality of VP populations, we differentiated and tested the four purified subsets with Matrigel tube-forming and Dil-acetylated-low density lipoprotein (Dil-Ac-LDL) uptake assays. As a group, EGM2-expanded CD31$^+$CD146$^+$ populations from hESC, CB-iPSC, and fibroblast-iPSC demonstrated significantly higher percentages of Dil-acetylated-low density lipoprotein$^+$ (Dil-Ac-LDL) uptake (Figure 1C). Although expanded CD31$^+$CD146$^-$ and CD31$^+$CD146$^+$ populations both formed organized microtubes in Matrigel (and with capillary-like lumens in collagen gels), CD31$^+$CD146$^+$ VP formed larger diameter, and more extensively branching vascular tubes (Figure 1D, Figure S8).

To confirm the vascular potential of putative VP populations *in vivo*, expanded cells from each FACS-purified group were resuspended in Matrigel and injected subcutaneously into NOD-SCID mice. Capacity for three-dimensional vessel formation was quantified two weeks later in Matrigel plugs. CD31$^+$CD146$^+$ VP populations expanded for 7–10 days in EGM2 proved most optimal for forming significantly greater numbers of large-diameter chimerized human-mouse blood vessels (>30 μm) in these Matrigel plugs (Figure 1E–F, Figure S7, S9). Chimerized vessels carried circulating murine blood within them, thus demonstrating successful anastomosis and developmental maturity.

CB-iPSCs Generated CD31$^+$CD146$^+$ VP with Higher Efficiency than Fibroblast-iPSC

To determine the differentiation efficiency of generating this novel VP population from hPSC, we differentiated 18 hPSC lines derived *via* various methods; this included 4 hESC

lines (H1, H7, H9, ES03), four viral fibroblast-iPSC lines (IMR90-1, IMR90-4, HUF3, HUF5), four 7F-episomal (7F-E) fibroblast-iPSC lines (7ta, WT2, WT4, SF-iPSC 6.1), and six episomal CB-iPSC lines (7F-E: 6.2, 6.13, 19.11; 4F-episomal (4F-E): E5C3, E12C5, E17C6). Although most hiPSC lines differentiated to the vascular lineage with efficiencies relatively comparable to hESC lines, CB-iPSC as a group produced significantly ($p<0.01$) higher frequencies of $CD31^+CD146^+$ VP cells than fibroblast-iPSC (Figure 2A). These hiPSC-derived VP populations displayed morphologies similar to neonatal EC (*e.g.*, human umbilical vein endothelial cells (HUVEC), and readily took up Dil-Ac-LDL and endothelial-specific Ulex-europaeus agglutinin[38] (UEA-1) (Figure 2B–D). There were no apparent quantitative differences in capacity to generate $CD31^+CD146^+$ VP between viral and episomal-derived fibroblast-iPSC, or as a function of passage number (data not shown). However, HF CB-iPSC VP possessed significantly higher capacities for Dil-Ac-LDL uptake than did fibroblast-iPSC VP, and with minimal hiPSC interline variability (Figure 2E). Purified CB-iPSC-VP expanded for several weeks also maintained higher expressions of VP markers (*e.g.*, CD31, CD146, KDR (VEGFR2), CD90, and CD144 (VE-Cadherin)), and stably maintained their capacity for generating branching, sprouting endothelial-pericytic micro-vascular tubes with capillary-like lumens in collagen gels (Figure 2F,G).

CB-iPSC-Derived VP Possessed Transcriptional Signatures with Closer Resemblance to VP Generated from hESC

To evaluate the molecular resemblance of embryonic hPSC-derived VP to adult vascular EC (*e.g.*, HUVEC and human microvascular endothelial cells (HMVEC)), we compared whole genome transcriptional signatures of adult EC to FACS-purified embryonic VP with Illumina expression microarrays. We computed unsupervised hierarchical clustering and principal component analysis (PCA) of global expression variance (34,680 genes) of FACS-purified and expanded $CD31^+CD146^+$ VP from hESC, CB-iPSC, Fibroblast-iPSC, *vs*. adult HUVEC, HMVEC, donor CB cells, donor fibroblasts, and undifferentiated hESC (Figure 3A, Figure S10). This global expression analysis did not sharply distinguish the VP generated from each hPSC class, but did demonstrate that embryonic VP from all hPSC sources were transcriptionally distinct from adult differentiated HUVEC/HMVEC.

A focused expression analysis of vascular lineage-specific genes by microarray revealed that VP generated from CB-iPSC shared more congruence in their vascular expression signatures[39] (Table S8) with hESC-VP than did VP from fibroblast-iPSC (Figure 3B, C). Interestingly, CB-iPSC-VP populations expressed higher transcript levels of endothelial-specific, perivascular/pericytic-specific genes (*e.g.*, PDGFRb. (CD140b)), and adhesion/migration-specific genes (e.g., integrin a5) than other hPSC classes (Figure 3B, Table S8). Quantitative real-time (qRT)-PCR expression analysis of key hemato-vascular genes (*e.g.*, CD31, CD34, von Willebrand factor (vWF), FLT1, TIE1, and TIE2) further confirmed the notion that embryonic hPSC-derived VP populations were more primitive than adult HUVEC (Figure 3D). For example, VP differentiated from hESC and CB-iPSC expressed higher transcript levels of immature endothelial progenitor markers such as TIE1 and TIE2, and lower expressions of mature endothelial transcripts (e.g., vWF) than adult endothelial cells.

To determine differential expression of genes in VP derived from either CB-iPSC or fibroblast-iPSC that distinguished them from VP derived from hESC, we conducted comparative bioinformatics analyses (Figure S11). These studies demonstrated that CB-iPSC-VP possessed significantly fewer (344) differentially expressed genes with hESC-derived VP than did VP generated from fibroblast-iPSC (628). A gene ontology (GO) analysis of the genes that were differentially expressed between fibroblast-derived VP and hESC-VP revealed systematic differences in fibroblast-iPSC-VP genes that regulate processes of developmental fate, signal transduction, cell adhesion, and cell growth/proliferation (Table S9). Taken together these genom-wide transcriptomic studies suggested that embryonic VP generated from CB-iPSC had fewer aberrant transcriptional patterns, and a significantly greater transcriptional resemblance to embryonic VP differentiated from hESC

CB-iPSC-VP Demonstrated Reduced Senescence and Sensitivity to DNA Damage

Previous studies with standard viral fibroblast-iPSC lines reported significantly diminished and highly variable directed differentiation to the vascular-endothelial lineage[29]. For example, differentiations of fibroblast-iPSC were characterized by poor growth and expansion of vascular-endothelial cells, with high rates of apoptosis and early senescence. To determine the functional quality of VP generated with our system, purified VP differentiated from hESC, fibroblast-iPSC, and CB-iPSC were expanded in EGM2 for up to 30 days (~4 passages) and senescent cells were quantified *via* β-galactosidase activity (Figure 4A). These studies revealed that CB-iPSC-VP maintained more enhanced proliferation, and significantly less senescence following expansion for several passages compared to fibroblast-iPSC-derived VP (Figure 4B). To further evaluate the nature of this relative resistance of CB-iPSC-VP to senescence, we probed the capacity of VP generated from the three classes of hPSC to maintain genomic integrity by assaying for sensitivity to double stranded DNA (dsDNA) damage following irradiation. Expression of p53 protein, which is normally activated briefly following DNA damage, was compared before and after 24 hours of 2Gy irradiation (Figure 4C, D). These studies revealed that p53 levels were relatively lower in expanded CB-iPSC-VP, suggesting a reduced sensitivity to irradiation-induced DNA damage compared to fibroblast-iPSC-VP. Interestingly, CB-iPSC-derived VP protein levels of RAD51, which also plays an important role in mediating repair from dsDNA damage following irradiation was also more comparable to hESC-derived VP (data not shown).

CB-iPSC-Derived VP Demonstrated Augmented Capacity for Homing and Engraftment into Retinal Vasculature of I/R-Damaged NOD-SCID Mice

To test the potential for *in vivo* ocular vessel engraftment of hiPSC-VP, we generated luciferase transgene-expressing hESC (H9), fibroblast-iPSC (IMR90-1), and CB-iPSC (6.2) lines representing the three major classes of hPSC being evaluated in this study (Figure S12). These luciferase-marked hPSC lines were differentiated to VP as described in Figure 1A. 50,000 luciferase^{+} human VP cells were injected directly into the vitreous body of NOD-SCID recipient eyes 2 days following I/R injury, and human cell engraftment in murine retina was evaluated at 3, 7, 14, 21, and 45 days later with anti-luciferase immunofluorescent staining (Figure 5A).

Interestingly, hPSC-derived $CD31^+CD146^-$ cells failed to migrate efficiently into I/R-damaged retina and home to blood vessels, and instead remained in the vitreous body, or adherent to the superficial layer of retina adjacent to vitreous (Figure 5B, right panel). In contrast, $CD31^+CD146^+$ VP migrated efficiently through the deep retinal layers, and homed and incorporated readily into blood vessels (Figure 5B, left panel; 5D, left panel). The migration distance and cell numbers of these $CD31^+CD146^+$ and $CD31^+CD146^-$ populations were quantitatively compared in serial retinal sections (Figure 5C). $CD31^+CD146^+$ cells not only migrated longer distances into the deeper retinal layers (~5-fold; $p<0.05$), but also higher numbers of cells were detected compared to $CD31^+CD146^-$ cells (~5-fold; $p<0.05$).

To evaluate mechanisms involved in enhanced retinal vessel homing of VP, we measured surface expression of CXCR4 (CD184), a critical chemokine that regulates cell migration[40]. $CD31^+CD146^+$ VP cells expressed higher levels of CXCR4 compared to $CD31^+CD146^-$ cells prior to vitreal injections (Figure S13). An analysis of migration of $CXCR4^+$ $CD31^+CD146^+$ VP cells into I/R-damaged eyes vs. normal non-injured control eyes revealed that homing to retinal vessels was dependent on vascular damage: $CD31^+CD146^+$ VP stayed adjacent to the internal limiting membrane (ILM) in eyes without injury signals (Figure 5D, right panel, Table 1). Following I/R injury, robust homing of $CD31^+CD146^+$ VP from both hESC and CB-iPSC into the retinal vasculatures was observed as early as three days following vitreal injection (Figure 5E, Table 1). In comparison, $CD31^+CD146^+$ VP from fibroblast-iPSC poorly homed and engrafted into retinal vessels in I/R-damaged eyes compared to CB-iPSC (Table 1).

CB-iPSC-VP Efficiently Engrafted into Damaged Retinal Blood Vessels Following Local and Systemic Injection for at Least 45 Days

In our I/R injury model, retinal vessel damage increases over time following I/R injury. To detect the sequential loss of murine host ECs, the retinal vasculature was stained with an antibody specific to mouse anti-CD31, and the vascular basement membrane was labeled with a murine anti-collagen type-IV antibody. This method demonstrated that blood vessel branches lost viable ECs as early as 7 days post I/R with the formation of acellular collagen tube-like capillary structures[4] (Figure S14). This damage was more severe in capillaries and veins presumably due to their higher collapsible or compressible nature under high intraocular pressure compared to arteries. Interestingly, VP injected into vitreous body initially assumed abluminal (pericytic) positions at early post-injection days 3 and 7 (Figure 5E arrows, Figure 6A–C arrows). Cryopreservation and sectioning of these retinas demonstrated stable enwrapping of the retinal blood vessels by human VP cells (Figure 6D–F, arrows).

To avoid the confusion of circulating cells appearing to be located in the lumen of blood vessels, mice were systemically perfused prior to the collection of retinas. At post-injection day 14, CB-iPSC-VP were clearly detected engrafting into both luminal endothelial and abluminal pericytic locations (Figure 6G, Figure S15A–B; Supplement Movie 1). Although hESC-VP could be found sporadically and non-specifically throughout neural retina, CB-iPSC-VP consistently demonstrated more specific engraftment into blood vessels (Figure

S15C–D, Table 1). At lower magnification of retinal flat-mounts, CB-iPSC-VP appeared to favor venous engraftment (blood vessels with larger diameter) than arteries (blood vessels with smaller diameter and more rigid walls) suggesting again that these cells preferentially migrated in response to injury signals (Figure S16, Supplementary Movie 2).

At post-systemic injection day 21, human cells were observed primarily in luminal locations in murine host retinal capillaries (Figure 6H, Figure S17, Supplementary movie 1). Chimeric capillaries on both linear (Figure S17A–C, E) as well as branch point (Figure S17C–D) vascular segments were detected, suggesting an injury-induced vasculogenesis, but that had no short-term impact on I/R-degenerated neuronal viability (Figure S18).

Finally, alternative injection of CB-iPSC-VP *via* orbital sinus or tail vein injection resulted in robust engraftment in endothelial or luminal cell positions that could be detected for at least 45 days (Figure 6I, Figure 7, Table 1). Intravenously injected human cells were detected and quantified in both the superficial capillary layer as well as the deeper retinal vascular networks (Figure 7). CB-iPSC-VP still homed to damaged retinal vessels in greater numbers (~2.4 fold for orbital sinus and ~1.6 fold for tail vein) in damaged eyes compared to uninjured normal eyes. This long-term engraftment is, to our knowledge, the most durable yet reported for injected hiPSC-derived vascular cells.

Discussion

We have identified a functional hPSC-derived embryonic VP population that can integrate long-term into ischemia-damaged mouse retinal vasculature. This study provides a preclinical model for evaluating the potential of patient-specific hiPSC-VP therapies for vascular degenerative disorders such as DR and BVO. Both ocular disorders progress to end stage death of retinal neurons and subsequent pathologic neovascularization. If VP could be used to repopulate acellular retinal capillaries and regenerate viable blood vessels, areas of ischemia could be reperfused, potentially avoiding end stage blinding complications. Such novel vascular therapies will require the efficient nonviral reprogramming of accessible somatic donor cells (*e.g.*, from skin or blood) that can generate hiPSC with superior vascular differentiation potential. Nonintegrated patient-specific hiPSC could be utilized to simultaneously generate both retinal neurons and VP for treating a variety of blinding disorders.

Our previous studies demonstrated that the barriers for efficient nonintegrated, nonviral pluripotency induction can be overcome by targeting highly accessible myeloid progenitors which are readily available from patient bone marrow, peripheral blood, or HLA-matched CB[31,32,41]. We have proposed that CB progenitors are especially attractive for pluripotency induction since they carry few somatic mutations, and could be used to create an HLA-defined stem cell bank for ocular regenerative medicine *via* worldwide networks of existing blood bank repositories[31,32]. Computational models predict that a small number of HLA-defined hPSC derived from existing cord and marrow banks could generate matches to serve the transplantation needs for the majority of the U.S. population[42]. Co-culturing human myeloid progenitors on patient-derived mesenchymal stromal layers, which our

reprogramming system employs, is a routine method already utilized in clinical trials in highly-reproducible, GMP-standardized conditions[43].

Although hESC and hiPSC share high molecular similarity, hiPSC generally possess more variable directed differentiation potencies than hESC[27–29,31]. Incomplete reprogramming and retention of donor-specific epigenetic memory have been proposed as etiologies for poor hiPSC differentiation potencies, including to vascular-endothelial lineages. In these studies, we found that HF CB-iPSC derived at very high efficiencies[31,32] possessed significantly augmented vascular potency compared to fibroblast-hiPSC derived via standard methods. These CB-iPSC generated $CD31^+CD146^+$ VP that were more akin molecularly to those generated from hESC, and with significantly fewer aberrant hiPSC-specific genes expressed that are likely due to transmitted reprogramming errors. Although previous studies demonstrated high senescence in vascular lineage cells generated from fibroblast-derived hiPSC[29], CB-iPSC-VP expanded more robustly in culture, possessed lower rates of culture senescence, and demonstrated more resistance to DNA damage than fibroblast-iPSC. Moreover, our *in vivo* engraftment results suggested that CB-iPSC-VP may possess advantages in survival, migration, and homing to damaged tissues in comparison to fibroblast-iPSC-VP. Derivation methods with more effective reprogramming capacities may greatly improve the final functional pluripotency of hiPSC, including to the vascular lineage. Further studies that explore the role of epigenetic memory will ultimately confirm if HF CB-iPSC will have greater clinical utility for generating multiple transplantable lineages (e.g. neural, vascular, retinal pigmented epithelium) for comprehensive regenerative therapy of blinding ocular diseases.

One important aspect of CB-iPSC-derived $CD31^+CD146^+$ VP was their efficient capacity to home to injured vessels. Despite damage to ischemic acellular capillaries, the basement membrane shared by EC and pericytes in ischemic retinal capillaries is normally spared. Although many growth factors regulate homing to sites of injury, the most likely stimulus is stromal derived factor-1 (SDF-1)/CXCR4-mediated migration[40]. We have previously demonstrated that the human retinal vasculature develops by specialized vasculogenesis, differentiation, and coalescence of angioblasts to form blood vessels at ~14 weeks gestation[44,45]. Retinal angioblasts during normal development, as well as the hiPSC-derived VP we have described, expressed robust levels of CXCR4 (the receptor for hypoxia-inducible SDF-1), thus presumably providing efficient homing of transplanted progenitors to hypoxic, damaged retinal vessels. As angioblasts migrate to the inner retina, they continue to express CXCR4 until they differentiate into the ECs that line patent retinal vessel lumens. SDF-1 is prominently localized to the innermost portion of retina during retinal vascular development and displays a gradient towards the outer retina[44]. Retinal angioblasts also expressed VEGFR-2/KDR and C-KIT similar to these embryonic VP. Thus, hPSC-derived $CD31^+CD146^+$ VP migration, homing, and engraftment in our I/R injury model likely recapitulate the hypoxic events during retinal development, when SDF/CXCR4 regulation is prominent.

Another important aspect of this study was the comparative demonstrations of transplanting hPSC-VP via intra-vitreal, orbital sinus, and intravenous administrations. When directly injected into vitreous, VP homed to injured blood vessels and engrafted primarily in

pericytic positions on the outside of host collagenous vascular tubes. In contrast, VP delivered intravenously engrafted primarily in endothelial positions. This behavior is reminiscent of early studies in developing retinal vasculature that suggested position in reference to the basement membrane determines the developmental fate of VP[45]. The future aim of selectively delivering hiPSC-derived EC or pericytes (or both) by targeting different routes to the damaged retina could have value in regenerating vascular segments in the diabetic retina where pericytes die prior to ECs before yielding acellular capillaries. Thus, this model establishes an important tool for evaluating the further development of clinically relevant hiPSC-based regenerative therapies for treatment of ischemic retinopathies.

Supplementary Material

Refer to Web version on PubMed Central for supplementary material.

Acknowledgments

We thank Dr. Takayuki Baba, Scott McLeod, Murilo Rodiriguez, Dr. Malia Edwards, Dr. Wayne Yu, and Karan Verma for technical support, and Dr. Jingxia Wang for statistical consultation. We are grateful to Ada Tam and Lee Blosser for their expertise in FACS. We are grateful to Alan Friedman for reading and editing the manuscript.

Funding Sources: This work was supported by grants from the NIH/NHLBI U01HL099775(ETZ) and U01HL100397(JC,RR-P), NIH/NEI R01-EY09357(GL), Research to Prevent Blindness unrestricted funds and EY01761-Wilmer Eye Institute (GL), NIH/NCI CA60441(JSH) and the Maryland Stem Cell Research Fund 2011-MSCRF-II-0008-00(ETZ); 2007-MSCRF-II-0379-00(ETZ); 2011-MSCRF-E-0023-00(GL); 2009-MSCRF-III-106570(TSP); 2007-MSCRFE-0110-00(RAF); 2009-MSCRFII-0082-00(RAF); 2011-MSCRFII-0023-00(FVR).

References

1. Paxhia MJ, Ting TD, Fekrat S. Ischemic central retinal vein occlusion and retinitis pigmentosa: Lower risk of neovascularization? Retina. 2001; 21:179–180. [PubMed: 11321148]
2. Awdeh RM, Elsing SH, Deramo VA, Stinnett S, Lee PP, Fekrat S. Vision-related quality of life in persons with unilateral branch retinal vein occlusion using the 25-item national eye institute visual function questionnaire. Br J Ophthalmol. 2010; 94:319–323. [PubMed: 19737736]
3. Cao J, McLeod S, Merges CA, Lutty GA. Choriocapillaris degeneration and related pathologic changes in human diabetic eyes. Arch Ophthalmol. 1998; 116:589–597. [PubMed: 9596494]
4. Zheng L, Gong B, Hatala DA, Kern TS. Retinal ischemia and reperfusion causes capillary degeneration: Similarities to diabetes. Invest Ophthalmol Vis Sci. 2007; 48:361–367. [PubMed: 17197555]
5. Kim SY, Johnson MA, McLeod DS, Alexander T, Otsuji T, Steidl SM, Hansen BC, Lutty GA. Retinopathy in monkeys with spontaneous type 2 diabetes. Invest Ophthalmol Vis Sci. 2004; 45:4543–4553. [PubMed: 15557466]
6. Joussen AM, Poulaki V, Le ML, Koizumi K, Esser C, Janicki H, Schraermeyer U, Kociok N, Fauser S, Kirchhof B, Kern TS, Adamis AP. A central role for inflammation in the pathogenesis of diabetic retinopathy. FASEB J. 2004; 18:1450–1452. [PubMed: 15231732]
7. Kim SY, Johnson MA, McLeod DS, Alexander T, Hansen BC, Lutty GA. Neutrophils are associated with capillary closure in spontaneously diabetic monkey retinas. Diabetes. 2005; 54:1534–1542. [PubMed: 15855343]
8. Joussen AM, Murata T, Tsujikawa A, Kirchhof B, Bursell SE, Adamis AP. Leukocyte-mediated endothelial cell injury and death in the diabetic retina. Am J Pathol. 2001; 158:147–152. [PubMed: 11141487]
9. D'Amore PA. Mechanisms of retinal and choroidal neovascularization. Invest Ophthalmol Vis Sci. 1994; 35:3974–3979. [PubMed: 7525506]

10. Glaser BM, D'Amore PA, Michels RG, Patz A, Fenselau A. Demonstration of vasoproliferative activity from mammalian retina. J Cell Biol. 1980; 84:298–304. [PubMed: 6155381]
11. Grant MB, Caballero S, Brown GA, Guthrie SM, Mames RN, Vaught T, Scott EW. The contribution of adult hematopoietic stem cells to retinal neovascularization. Adv Exp Med Biol. 2003; 522:37–45. [PubMed: 12674209]
12. Sengupta N, Caballero S, Mames RN, Butler JM, Scott EW, Grant MB. The role of adult bone marrow-derived stem cells in choroidal neovascularization. Invest Ophthalmol Vis Sci. 2003; 44:4908–4913. [PubMed: 14578416]
13. Sengupta N, Afzal A, Caballero S, Chang KH, Shaw LC, Pang JJ, Bond VC, Bhutto I, Baba T, Lutty GA, Grant MB. Paracrine modulation of cxcr4 by igf-1 and vegf: Implications for choroidal neovascularization. Invest Ophthalmol Vis Sci. 2010; 51:2697–2704. [PubMed: 20007826]
14. Lu SJ, Feng Q, Caballero S, Chen Y, Moore MA, Grant MB, Lanza R. Generation of functional hemangioblasts from human embryonic stem cells. Nat Methods. 2007; 4:501–509. [PubMed: 17486087]
15. Friedlander M, Dorrell MI, Ritter MR, Marchetti V, Moreno SK, El-Kalay M, Bird AC, Banin E, Aguilar E. Progenitor cells and retinal angiogenesis. Angiogenesis. 2007; 10:89–101. [PubMed: 17372851]
16. Caballero S, Sengupta N, Afzal A, Chang KH, Li Calzi S, Guberski DL, Kern TS, Grant MB. Ischemic vascular damage can be repaired by healthy, but not diabetic, endothelial progenitor cells. Diabetes. 2007; 56:960–967. [PubMed: 17395742]
17. Brunner S, Hoellerl F, Schmid-Kubista KE, Zeiler F, Schernthaner G, Binder S, Schernthaner GH. Circulating angiopoietic cells and diabetic retinopathy in type 2 diabetes mellitus, with or without macrovascular disease. Invest Ophthalmol Vis Sci. 2011; 52:4655–4662. [PubMed: 21398276]
18. Wang ZZ, Au P, Chen T, Shao Y, Daheron LM, Bai H, Arzigian M, Fukumura D, Jain RK, Scadden DT. Endothelial cells derived from human embryonic stem cells form durable blood vessels in vivo. Nat Biotechnol. 2007; 25:317–318. [PubMed: 17322871]
19. Ferreira LS, Gerecht S, Shieh HF, Watson N, Rupnick MA, Dallabrida SM, Vunjak-Novakovic G, Langer R. Vascular progenitor cells isolated from human embryonic stem cells give rise to endothelial and smooth muscle like cells and form vascular networks in vivo. Circ Res. 2007; 101:286–294. [PubMed: 17569886]
20. Li Z, Wu JC, Sheikh AY, Kraft D, Cao F, Xie X, Patel M, Gambhir SS, Robbins RC, Cooke JP. Differentiation, survival, and function of embryonic stem cell derived endothelial cells for ischemic heart disease. Circulation. 2007; 116:146–154.
21. Rufaihah AJ, Huang NF, Jame S, Lee JC, Nguyen HN, Byers B, De A, Okogbaa J, Rollins M, Reijo-Pera R, Gambhir SS, Cooke JP. Endothelial cells derived from human iPSCs increase capillary density and improve perfusion in a mouse model of peripheral arterial disease. Arterioscler Thromb Vasc Biol. 2011; 31:e72–e79. [PubMed: 21836062]
22. Dar A, Domev H, Ben-Yosef O, Tzukerman M, Zeevi-Levin N, Novak A, Germanguz I, Amit M, Itskovitz-Eldor J. Multipotent vasculogenic pericytes from human pluripotent stem cells promote recovery of murine ischemic limb. Circulation. 2012; 125:87–99. [PubMed: 22095829]
23. Park TS, Zambidis ET, Lucitti JL, Logar A, Keller BB, Peault B. Human embryonic stem cell-derived hematoendothelial progenitors engraft chicken embryos. Exp Hematol. 2008; 37:31–41. [PubMed: 18954935]
24. Zambidis ET, Park TS, Yu W, Tam A, Levine M, Yuan X, Pryzhkova M, Peault B. Expression of angiotensin-converting enzyme (CD143) identifies and regulates primitive hemangioblasts derived from human pluripotent stem cells. Blood. 2008; 112:3601–3614. [PubMed: 18728246]
25. Grant MB, May WS, Caballero S, Brown GA, Guthrie SM, Mames RN, Byrne BJ, Vaught T, Spoerri PE, Peck AB, Scott EW. Adult hematopoietic stem cells provide functional hemangioblast activity during retinal neovascularization. Nat Med. 2002; 8:607–612. [PubMed: 12042812]
26. Peters A, Burridge PW, Pryzhkova MV, Levine MA, Park TS, Roxbury C, Yuan X, Peault B, Zambidis ET. Challenges and strategies for generating therapeutic patient-specific hemangioblasts and hematopoietic stem cells from human pluripotent stem cells. Int J Dev Biol. 2010; 54:965–990. [PubMed: 20563986]

27. Ramos-Mejia V, Montes R, Bueno C, Ayllon V, Real PJ, Rodriguez R, Menendez P. Residual expression of the reprogramming factors prevents differentiation of iPSC generated from human fibroblasts and cord blood CD34+ progenitors. PLoS ONE. 2012; 7:e35824. [PubMed: 22545141]
28. Miura K, Okada Y, Aoi T, Okada A, Takahashi K, Okita K, Nakagawa M, Koyanagi M, Tanabe K, Ohnuki M, Ogawa D, Ikeda E, Okano H, Yamanaka S. Variation in the safety of induced pluripotent stem cell lines. Nat Biotechnol. 2009; 27:743–745. [PubMed: 19590502]
29. Feng Q, Lu SJ, Klimanskaya I, Gomes I, Kim D, Chung Y, Honig GR, Kim KS, Lanza R. Hemangioblastic derivatives from human induced pluripotent stem cells exhibit limited expansion and early senescence. Stem Cells. 2009; 28:704–712. [PubMed: 20155819]
30. Yu J, Hu K, Smuga-Otto K, Tian S, Stewart R, Slukvin II, Thomson JA. Human induced pluripotent stem cells free of vector and transgene sequences. Science. 2009; 324:797–801. [PubMed: 19325077]
31. Burridge PW, Thompson S, Millrod MA, Weinberg S, Yuan X, Peters A, Mahairaki V, Koliatsos VE, Tung L, Zambidis ET. A universal system for highly efficient cardiac differentiation of human induced pluripotent stem cells that eliminates interline variability. PLoS ONE. 2011; 6:e18293. [PubMed: 21494607]
32. Park TS, Huo JS, Peters A, Talbot CC Jr, Verma K, Zimmerlin L, Kaplan IM, Zambidis ET. Growth factor-activated stem cell circuits and stromal signals cooperatively accelerate non-integrated ipsc reprogramming of human myeloid progenitors. PLoS ONE. 2012; 7:e42838. [PubMed: 22905176]
33. Park TS, Zimmerlin L, Zambidis ET. Efficient and simultaneous generation of hematopoietic and vascular progenitors from human induced pluripotent stem cells. Cytometry A. 2012; 1:114–126. [PubMed: 22736485]
34. Park, TS.; Burridge, PETZ. Lineage-specific differentiation of human embryonic stem cells and induced pluripotent stem cells. Patrick J Marton: Springer Protocols; 2011. Chapter 24: Generation of multipotent CD34+CD45+ hematopoietic progenitors from human induced pluripotent stem cells.
35. Zambidis ET, Peault B, Park TS, Bunz F, Civin CI. Hematopoietic differentiation of human embryonic stem cells progresses through sequential hematoendothelial, primitive, and definitive stages resembling human yolk sac development. Blood. 2005; 106:860–870. [PubMed: 15831705]
36. Crisan MA, Yap S, Casteilla L, Chen C-W, Corselli M, Park TS, Andriolo G, Sun B, Zhang L, Norotte C, Teng PN, Traas J, Schugar R, Deasy BM, Badylak S, Buhring HS, Giacobino JP, Lazzari L, Huard J, Peault B. A perivascular origin for mesenchymal stem cells in multiple human organs. Cell Stem Cell. 2008; 3:301–313. [PubMed: 18786417]
37. Park TS, Gavina M, Chen CW, Sun B, Teng PN, Huard J, Deasy BM, Zimmerlin L, Peault B. Placental perivascular cells for human muscle regeneration. Stem Cells Dev. 2011; 20:451–463. [PubMed: 20923371]
38. Rehman J, Li J, Orschell CM, March KL. Peripheral blood"endothelial progenitor cells" are derived from monocyte/macrophages and secrete angiogenic growth factors. Circulation. 2003; 107:1164–1169. [PubMed: 12615796]
39. Choi KD, Vodyanik MA, Togarrati PP, Suknuntha K, Kumar A, Samarjeet F, Probasco MD, Tian S, Stewart R, Thomson JA, Slukvin II. Identification of the hemogenic endothelial progenitor and its direct precursor in human pluripotent stem cell differentiation cultures. Cell Rep. 2012
40. Gupta SK, Lysko PG, Pillarisetti K, Ohlstein E, Stadel JM. Chemokine receptors in human endothelial cells. Functional expression of CXCR4 and its transcriptional regulation by inflammatory cytokines. J Biol Chem. 1998; 273:4282–4287. [PubMed: 9461627]
41. Okita K, Yamakawa T, Matsumura Y, Sato Y, Amano N, Watanabe A, Goshima N, Yamanaka S. An efficient non-viral method to generate integration-free human ips cells from cord blood and peripheral blood cells. Stem Cells. 2012; 31:458–66. [PubMed: 23193063]
42. Taylor CJ, Bolton EM, Pocock S, Sharples LD, Pedersen RA, Bradley JA. Banking on human embryonic stem cells: Estimating the number of donor cell lines needed for HLA matching. Lancet. 2005; 366:2019–2025. [PubMed: 16338451]
43. de Lima M, McNiece I, Robinson SN, Munsell M, Eapen M, Horowitz M, Alousi A, Saliba R, McMannis JD, Kaur I, Kebriaei P, Parmar S, Popat U, Hosing C, Champlin R, Bollard C,

Molldrem JJ, Jones RB, Nieto Y, Andersson BS, Shah N, Oran B, Cooper LJ, Worth L, Qazilbash MH, Korbling M, Rondon G, Ciurea S, Bosque D, Maewal I, Simmons PJ, Shpall EJ. Cord-blood engraftment with ex vivo mesenchymal-cell coculture. N Engl J of Med. 2012; 367:2305–2315. [PubMed: 23234514]

44. Hasegawa T, McLeod DS, Prow T, Merges C, Grebe R, Lutty GA. Vascular precursors in developing human retina. Invest Ophthalmol Vis Sci. 2008; 49:2178–2192. [PubMed: 18436851]
45. McLeod DS, Hasegawa T, Prow T, Merges C, Lutty G. The initial fetal human retinal vasculature develops by vasculogenesis. Dev Dyn. 2006; 235:3336–3347. [PubMed: 17061263]

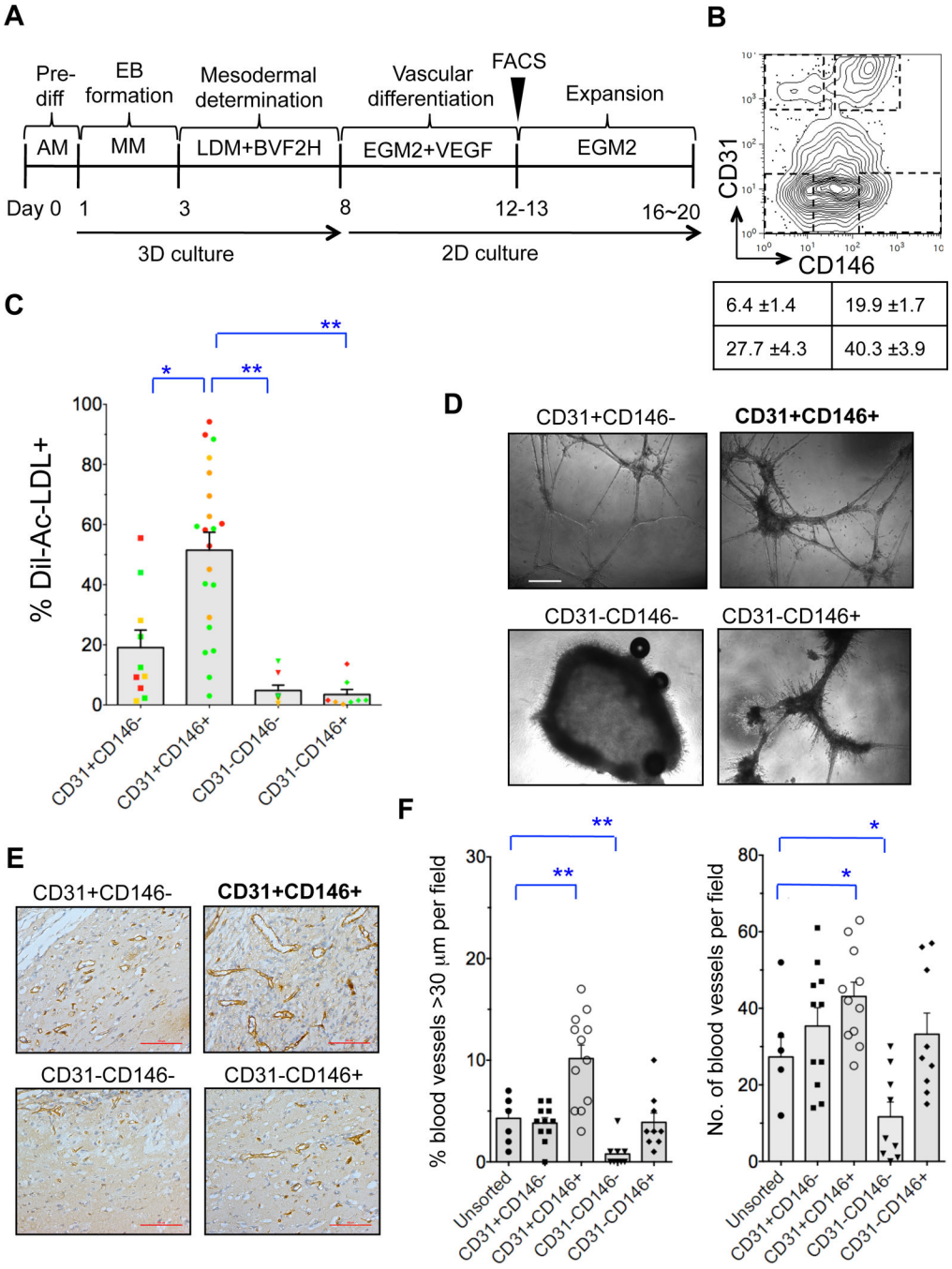

Figure 1.

Efficient generation of embryonic VP populations from hPSC. **A**, Schema for vascular differentiation and expansion of VP. **B**, Flow cytometry plot of day 8 hEB cells from H9-hESC following expansion in EGM2 for 4 days. The average percentage of four indicated quadrants ± SEM is shown (*n*=13 experiments). **C**, Percentage Dil-Ac-LDL uptake (Mean ± SEM) of FACS-purified and EGM2-expanded populations differentiated from two hESC lines (gold), three CB-iPSC lines (red) and six Fibro-iPSC lines (green). Each data point represents an independent, replicate experiment. **D**, *In vitro* Matrigel assays of purified and

expanded populations. Scale = 500 μm. **E**, Representative Matrigel plugs consisted of vascular structures formed by indicated CB-iPSC-6.2 hEB-derived populations, and immunostained with anti-CD31 (brown). Scale bars =100 μm. **F**, Measurements in Matrigel plug sections: (left panel) percentages of blood vessels >30 μm diameter per microscopic field (mean ±SEM); (right panel) total number of blood vessels per microscopic field (mean ±SEM) (Two-tailed t-tests, *: $p < 0.05$, **: $p < 0.01$).

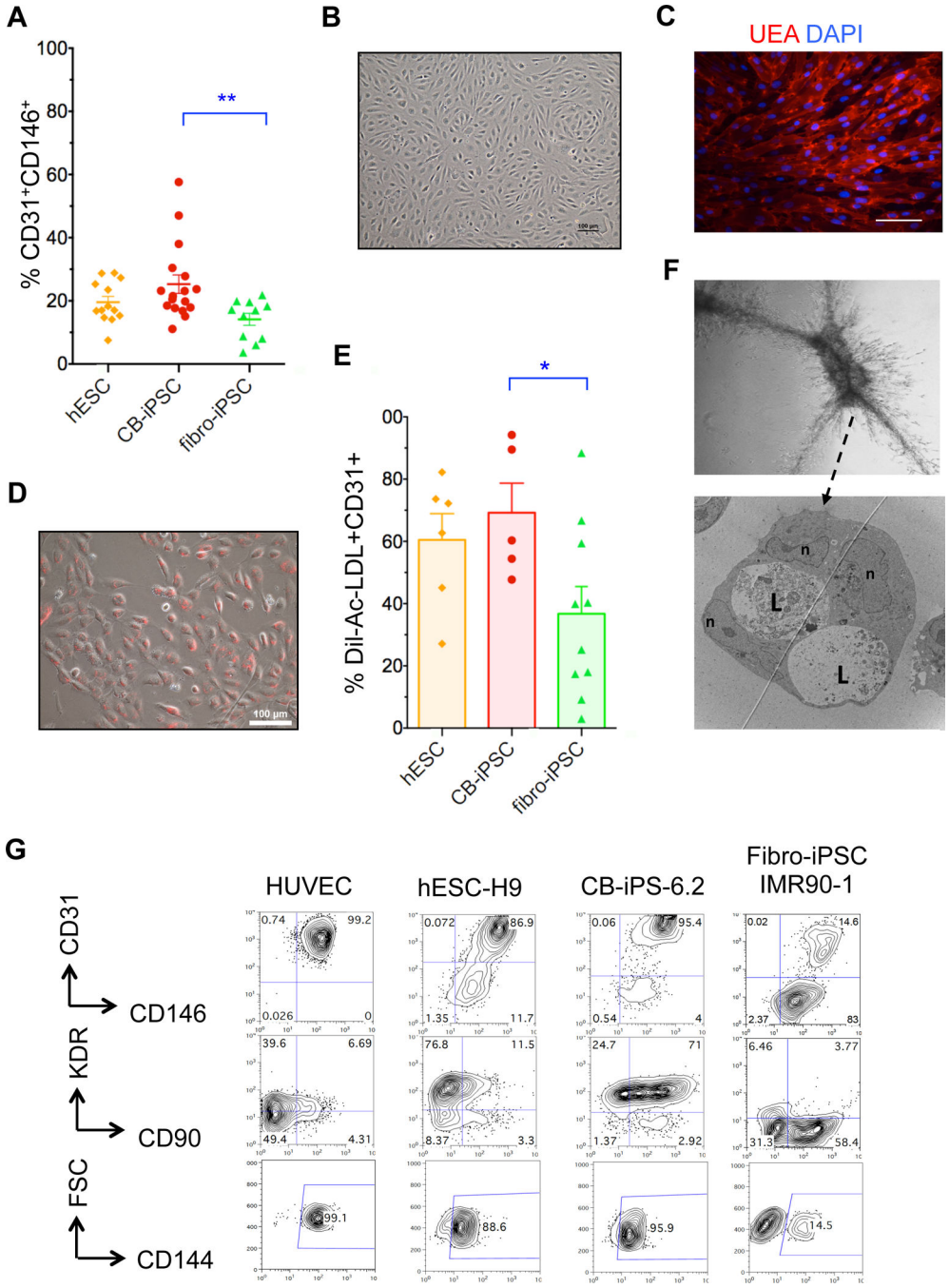

Figure 2.

Characterization of VP generated from hPSC. **A**, Efficiency of hEB differentiation (%mean ± SEM) of hPSC to $CD31^+CD146^+$ VP. Data are from four hESC lines (H1, H7, H9, ES03; *n*=13 experiments (gold)), eight fibroblast-iPSC lines (IMR90-1, IMR90-4, HUF3, HUF5, 7ta, WT2, WT4, fF6.1); *n*=11 experiments (green)), and six CB-iPSC lines (6.2, 6.13, 19.11, E5C3, E12C5, E17C6; *n*=17 experiments (red)). Two-tailed t-tests: **: p <0.01. **B**, Phase contrast image of FACS-purified, expanded $CD31^+CD146^+$ VP cells differentiated from CB-iPSC-6.2; **C**, with Ulex europaeus agglutinin (UEA) and DAPI co-staining **D**, and with

Dil-Ac-LDL uptake staining **E**, Percentage Dil-Ac-LDL uptake (mean ± SEM) of expanded $CD31^{+}CD146^{+}$ VP from individual differentiations of hESC (gold), CB-iPSC (red), and fibroblast-iPSC (green). Mann-Whitney tests: *: $p<0.05$. **F**, TEM image CB-iPSC-derived VP forming vascular tubes in collagen gel via cooperating endothelial and pericytic-like cells; all border on lumens and are potential EC in apparent bifurcation. L: lumen, n: nuclei. **G**, Representative surface marker analyses of FACS-purified/expanded hPSC-derived $CD31^{+}CD146^{+}$ VP and HUVEC.

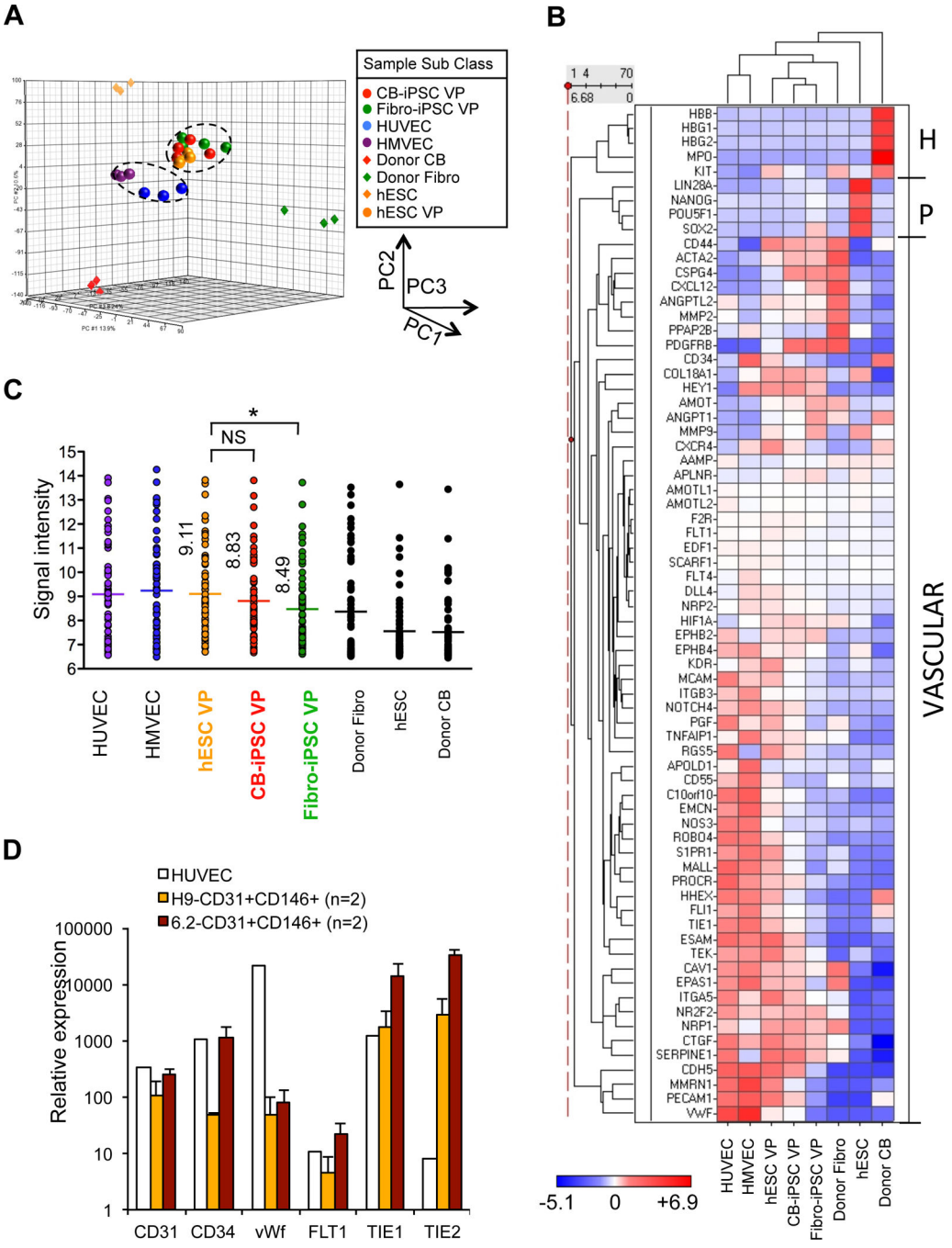

Figure 3.

Expression signatures of hPSC-derived VP. **A**, PCA of genome-wide expression signatures for indicated samples of embryonic $CD31^{+}CD146^{+}$ VP generated from hESC, CB-iPSC, and fibroblast-iPSC; adult endothelial cells (HUVEC, HMEC); hiPSC donor cells; hESC lines. Data were generated from samples in Figure S10. Pearson coefficient R^2 for hESC-VP vs. CB-iPSC-VP = 0.974; hESC-VP vs. fibroblast-iPSC-VP = 0.958. **B**, Heatmap-dendrogram of Ilumina expression array data of the vascular lineage-specific genes indicated. Individual RNA samples from independent differentiations were obtained from

HUVEC (*n*=3), HMVEC (*n*=3), hESC-VP (*n*=4), CB-iPSC-VP (*n*=4), fibroblast-iPSC-VP (*n*=4), donor fibroblast (Fibro, *n*=3), hESC (*n*=3), and donor CB (n=3). H: hematopoietic-specific genes, P: pluripotency-specific genes, VASCULAR: vascular lineage-specific genes. **C**, Quantitation of expression of vascular lineage-specific genes in **B**. Mean value of the gene signal intensity is shown (*: $p<0.05$; mean expression among hESC-VP, CB-iPSC-VP and Fib-iPSC-VP differed significantly (one-way ANOVA $p = 0.001$). Fib-iPSC-VP also significantly differed by individual comparison than hESC-VP ($p = 0.0002$, Bonferroni correction threshold $p < 0.016$), while CB-iPSC-VP vs. hESC-VP did not ($p = 0.09$). List of genes analyzed: Table S8. **D**, Q-RT-PCR analysis of $CD31^{+}CD146^{+}$ VP from hESC-H9, CB-iPSC-6.2, and HUVEC. Relative expression of CD31, CD34, vWF, FLT1, TIE1, and TIE2 of replicate samples was normalized to expression in undifferentiated hESC-H9 (*n*=2 experiments).

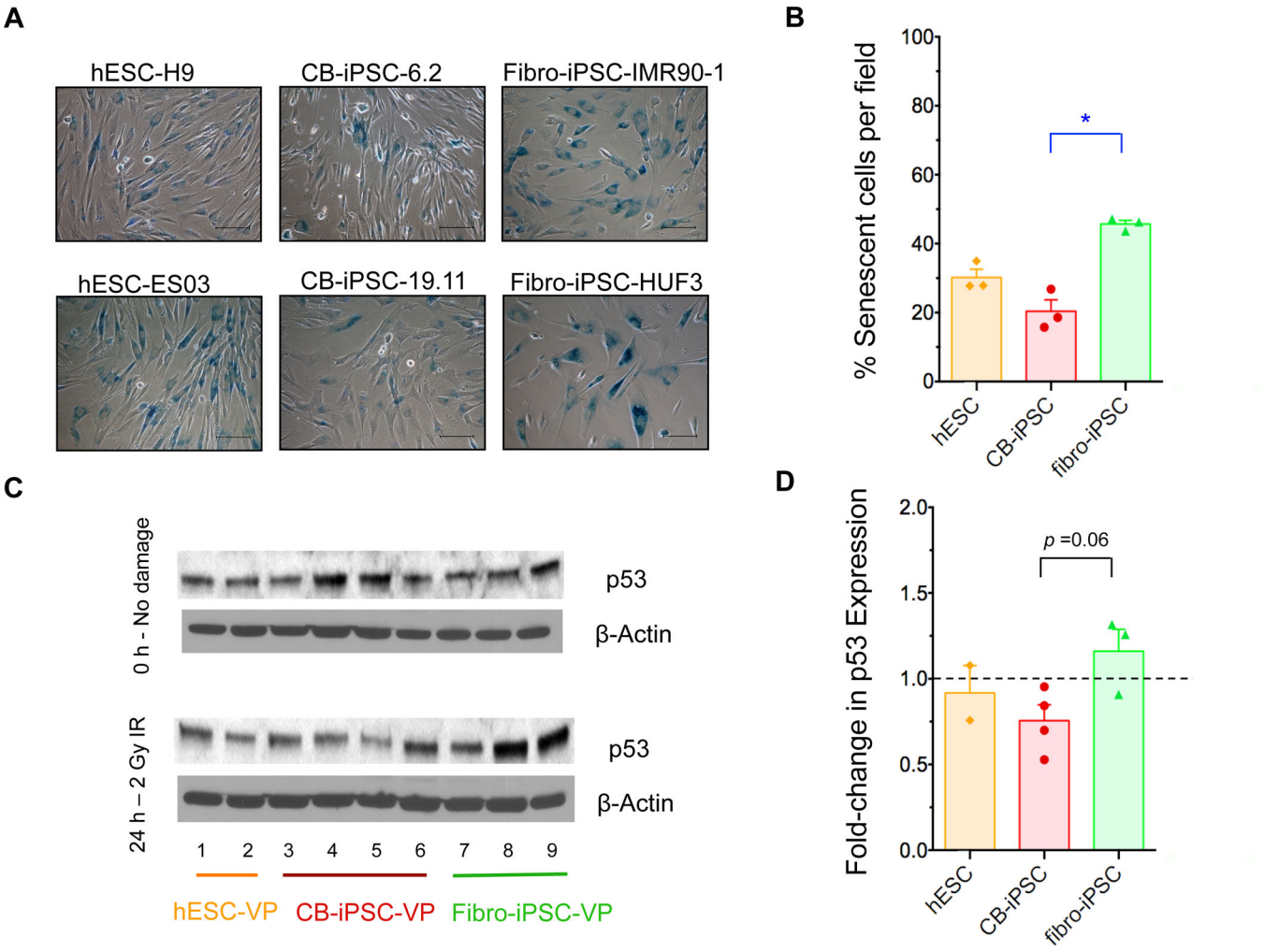

Figure 4.

Senescence and DNA damage sensitivity of expanded VP. **A**, Representative β-galactosidase senescence staining in hPSC classes; legend symbols are as before. Scale bars = 100 μm. **B**, % senescent cells (mean ±SEM of *n*=12 microscopic fields per each line of each hPSC class; *n*=3 per class). **C**. Western blots of p53 expression before, and 24 hours following 2Gy irradiation of VP from 1: H9 (p46), 2: ES03 (p88), 3: 6.2 (P20), 4: 6.2 (P23), 5: 19.11 (P19), 6: E17C6 (P29), 7: HUF3 (P44), 8: IMR90-1 (P71), 9: IMR90-1 (p72). **D**, Fold percent change in p53 protein expression levels by Western blot densitometry; >1.0 (increase) or <1.0 (decrease) above baseline). Two-tailed t-tests *: $p<0.05$.

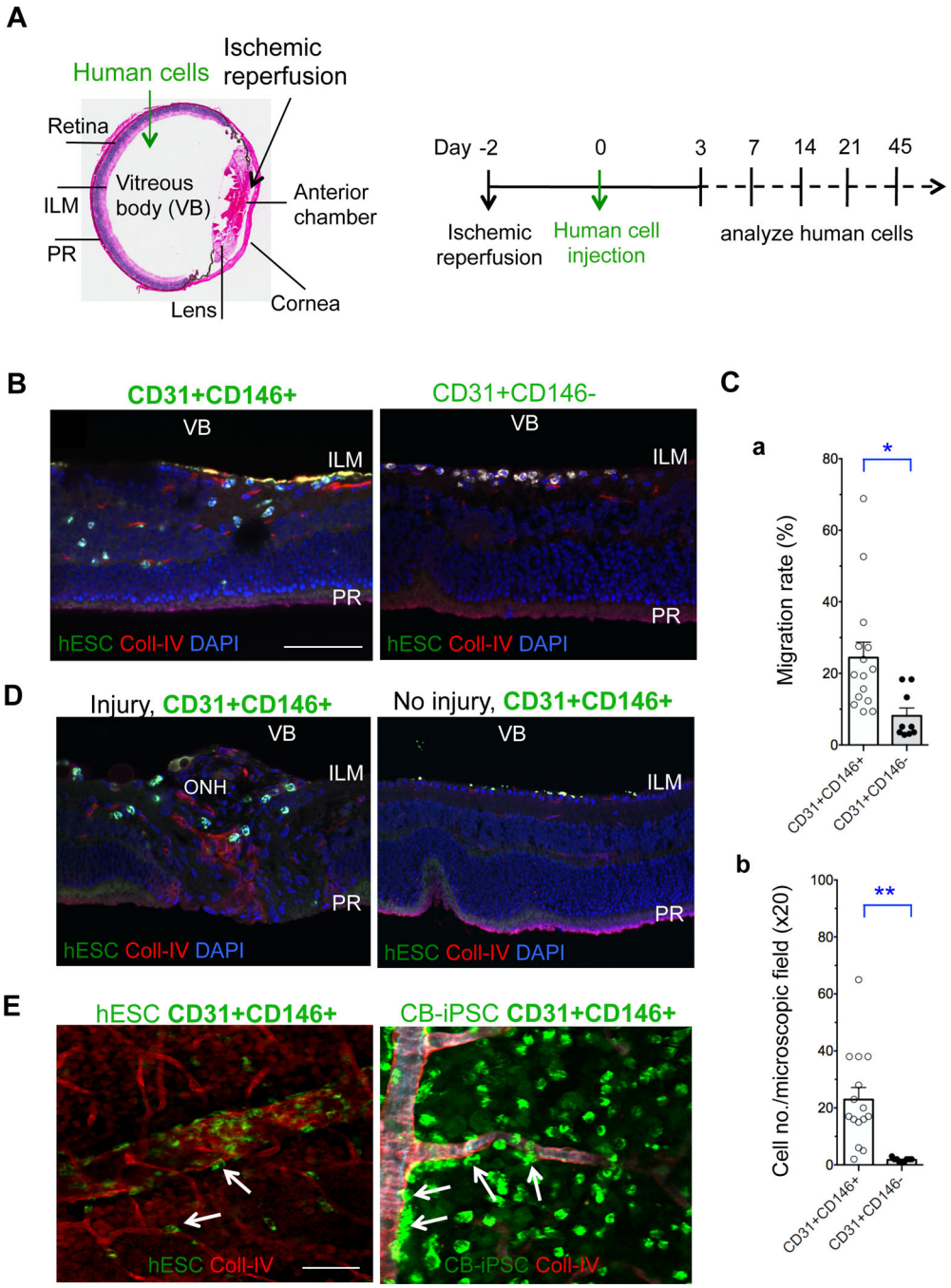

Figure 5.

In vivo migration, homing, and engraftment of luciferase-transgenic VP cells into I/R-damaged mouse retina. **A**, Experimental design for quantifying human VP engraftment into NOD-SCID mouse retinas. (Left panel) Anatomy of mouse eye indicating I/R location at anterior chamber and site of human cell injections into vitreous body. (Right panel) Timeline of *in vivo* engraftment analysis. **B**, Representative immuno-fluorescent retinal sections of I/R-damaged eyes injected with hESC-luciferase-transgenic (green) $CD31^{+}CD146^{+}$ VP (left) and $CD31^{+}CD146^{-}$ (right) cells at 3 days post-injection.

$CD31^+CD146^+$ cells readily migrated into deep retinal layers whereas $CD31^+CD146^-$ cells remained primarily in vitreous. (VB: vitreous body, ILM: internal limiting membrane, PR: photoreceptor) **C**, Quantification of (a) cell migration into retina and (b) number of engrafted human cells visualized per retinal cross sections following injection of hESC derived $CD31^+CD146^+$ VP and $CD31^+CD146^-$ cells (n=15 and 9 sections evaluated, respectively; two-tailed t-tests: * $p<0.005$; ** $p<0.001$). **D**, $CD31^+CD146^+$ hESC-VP injected to I/R-damaged (injury, left) and normal eye (no injury, right) demonstrating that cells do not migrate into retinal layers without injury signals. (ONH: optic nerve head) **E**, $CD31^+CD146^+$ hESC-VP (left) and $CD31^+CD146^+$ CB-iPSC-VP (right) engrafted into both venules and micro-capillaries (arrows) in this flat mount retina at post-injection day 3. Scale bars 50 μm.

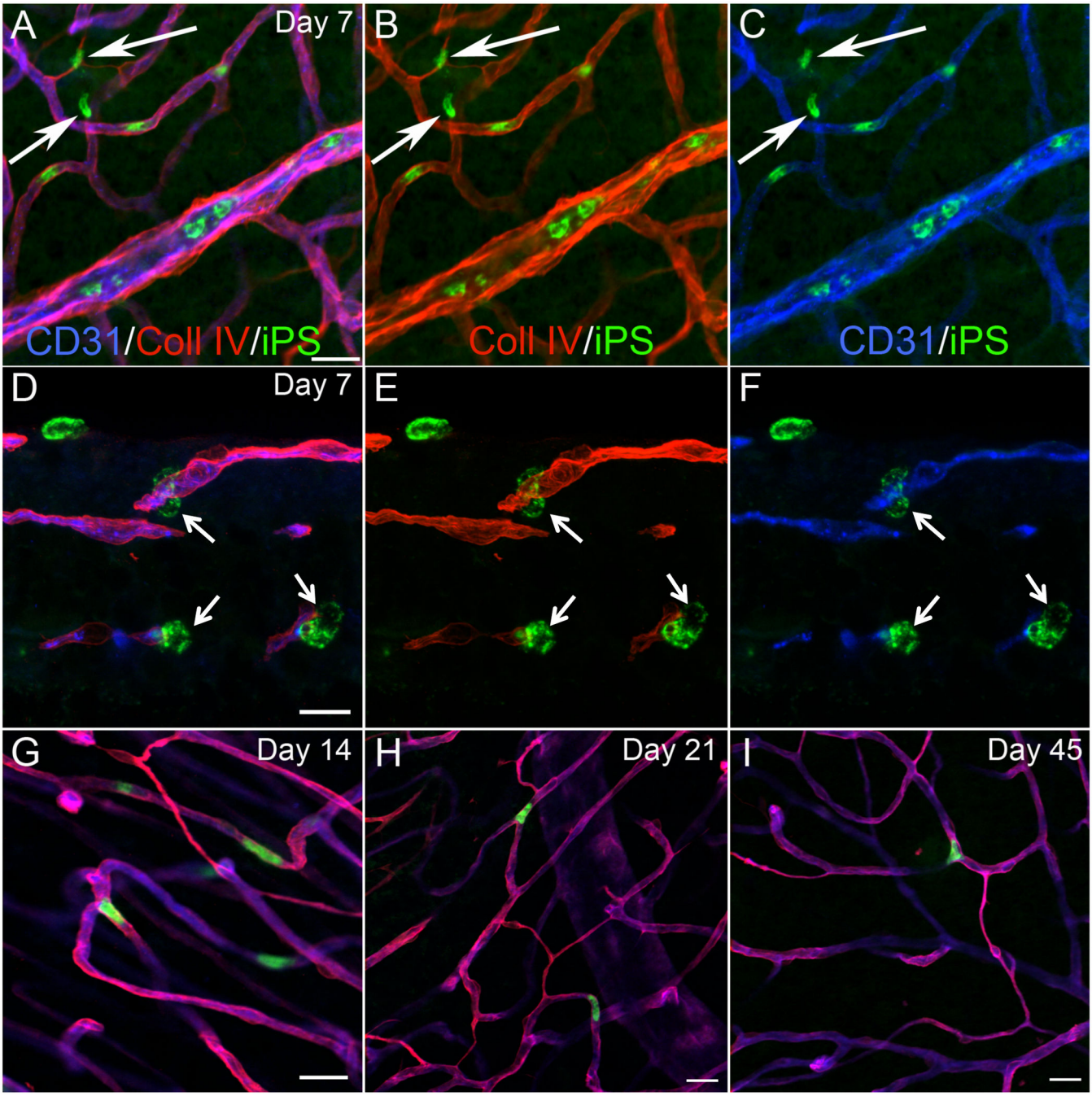

Figure 6.

In vivo engraftment of CB-iPSC-VP into retinal vasculature. Luciferase-transgenic human VP were injected directly into the eye (intra-vitreal) (**A–H**), or systemically IV (orbital sinus) (**I**). **G**, Transgenic CB-iPSC-VP (green) homed to both damaged capillaries (arrows), and larger blood vessels (retinal flat mounts). **C**, Damaged host vessels lacked murine ECs (lack of blue signal from anti-mouse CD31), but their Coll IV^{+} basement membranes remained intact (red). **D–F**, Human cells (green) were often observed in retinal cross-sections at pericytic positions surrounding host murine ECs (blue) in capillaries. Engrafted

human CB-iPSC-VP detected in murine retina at 14 days (**G**), 21 days (**H**), and 45 days (**I**) post injection. The degree of damage was more severe and the density of functional blood vessels was reduced with time following I/R. Scale bars are 20 μm (**A**, **G–I**) and 10 μm (**D**). Shown are representative experiments from Table 1.

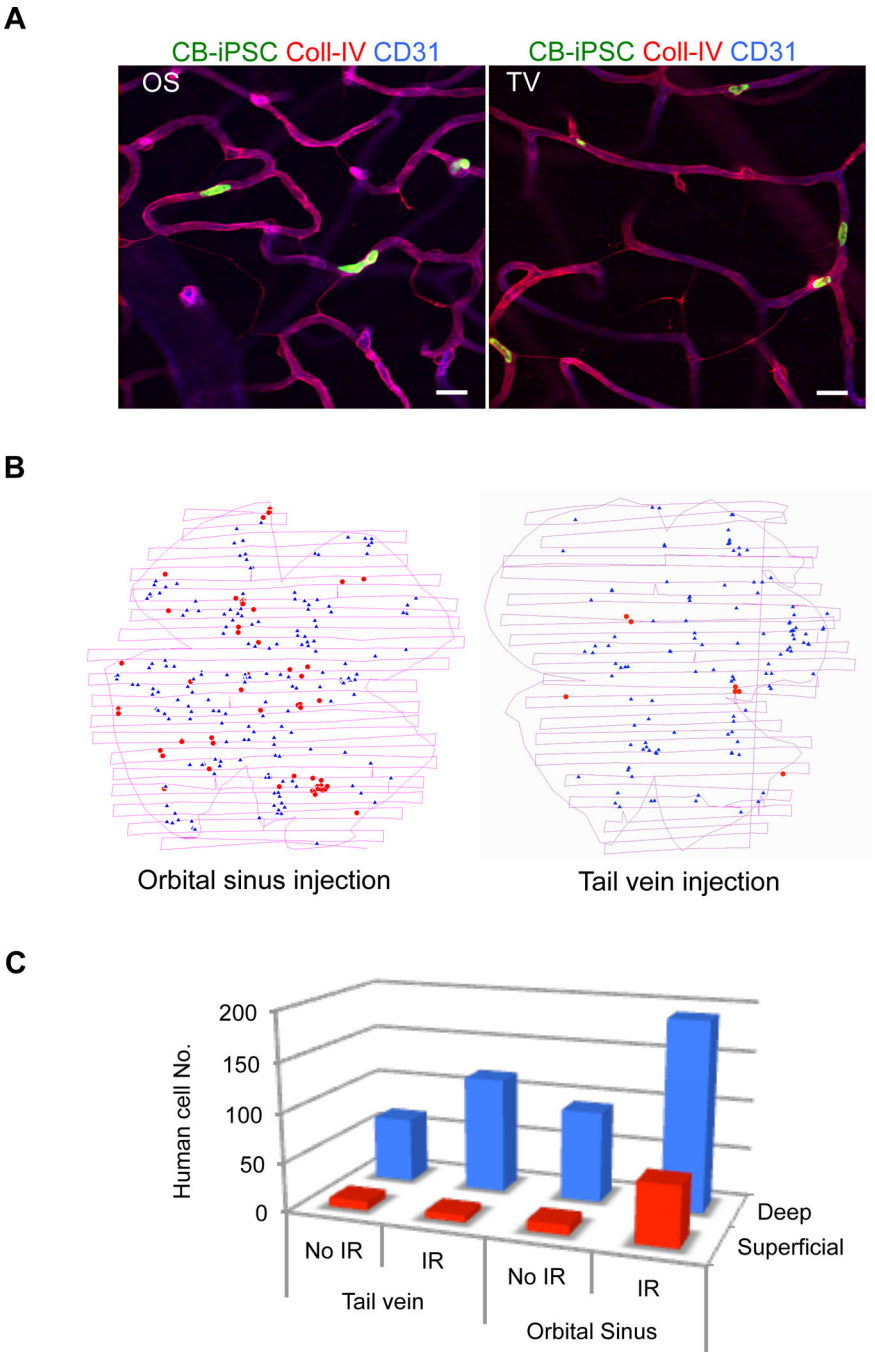

Figure 7.

Quantification of human VP engraftment into murine retinal vasculature. **A**, Representative experiments (from Table 1) demonstrating CB-iPSC-VP (green) engrafting into murine vessels following orbital sinus (OS) or tail-vein (TV) injections. Scale bars = 20 μm. **B**, Representative experiments showing detection of CB-iPSC-VP injected *via* orbital sinus (left) or tail vein (right). Retinas were harvested at post-injection day 7, and whole flat mount retinas were scanned and human cells quantified in superficial (near vitreous body, red) and deep retinal vasculatures (blue) layers. **C**, Representative quantification of a retinal

engraftment experiment demonstrated that systemic injections attracted higher numbers of homing $CD31^{+}CD146^{+}$ VP into damaged deep retinal blood vessels (OS>TV).

Table 1

Summary of *in vivo* I/R-damaged retinal vessel engraftment of VP generated from hESC, CB-iPSC, and fibroblast-iPSC *via* local vitreous body or systemic IV tail vein injections.

Intra-vitreal injection of CD31+CD146+ cells																		
Post-injection days	**hESC-H9**						**CB-iPSC-6.2**						**Fibroblast-iPSC-IMR90-1**					
	No I/R			**I/R**			**No I/R**			**I/R**			**No I/R**			**I/R**		
	V	**R**	***n***	**V**	**R**	***n***	**V**	**R**	***n***	**V**	**R**	***n***	**V**	**R**	***n***	**V**	**R**	***n***
Day 3	+	−	8	+	++	10	+	−	10	+	+	11	+	−	2	+	−	2
Day 7	+	−	7	+	+	7	+	−	7	−	++	8	+	−	3	+	+	3
Day 14	+/F	−	5	−	−	5	+	−	5	−	++	7	ND			ND		
Day 21	−	−/+	6	−	−/+	6	ND			−	++	2	ND			ND		

Tail vein injection of CD31+CD146+ cells				
Post-injection days	**hESC-H9**		**CB-iPSC-6.2**	
	I/R		**I/R**	
	R	***n***	**R**	***n***
Day 7	ND		++	4
Day 14	ND		++	14
Day 21	+	3	++	3
Day 45	ND		+	2

I/R ischemia-reperfusion
V Cells detected in vitreous body
R Cells engrafted in retinal blood vessels

− zero cells detected
+ 1−2 cells detected engrafted per microscopic field
++ >2 cells detected engrafted per microscopic field
F Fragmented, nonviable cells detected
n number of independent experiments
ND Not done